Lattice dynamics of wurtzite and rocksalt AlN under high pressure: Effect of compression on the crystal anisotropy of wurtzite-type semiconductors

Francisco Javier Manjón*
Departamento de Física Aplicada-IDF-MALTA Consolider Team, Universitat Politècnica de València, Camino de Vera s/n, 46022 Valencia, Spain

Daniel Errandonea
Departamento de Física Aplicada-ICMUV-MALTA Consolider Team, Universitat de València, C/. Dr. Moliner 50, Burjassot, 46100 Valencia, Spain

Aldo Humberto Romero
CINVESTAV, 76230 Querétaro, Mexico

Núria Garro
Fundació General de la Universitat de València-ICMUV, Universitat de València, Polígon La Coma s/n, 46980 Paterna, Spain

Jorge Serrano
ICREA–Departamento de Física Aplicada, EPSC, Universitat Politècnica de Catalunya, Avinguda Canal Olimpic 15, E-08860 Castelldefels, Spain

Martin Kuball
H.H. Wills Physics Laboratory, University of Bristol, Bristol BS8 1TL, United Kingdom
(Received 24 April 2007; revised manuscript received 17 April 2008; published 16 May 2008)

Raman spectra of aluminum nitride (AlN) under pressure have been measured up to 25 GPa, i.e., beyond the onset of the wurtzite-to-rocksalt phase transition around 20 GPa. The experimental pressure coefficients for all the Raman-active modes of the wurtzite phase are reported and compared to those obtained from *ab initio* lattice dynamical calculations, as well as to previous experimental and theoretical results. The pressure coefficients of all the Raman-active modes in wurtzite-type semiconductors (AlN, GaN, InN, ZnO, and BeO), as well as the relatively low bulk modulus and phase transition pressure in wurtzite AlN, are discussed in the light of the pressure dependence of the structural crystal anisotropy in wurtzite semiconductors. On pressure release, AlN partially returns to the wurtzite phase below 1.3 GPa but the presence of a rocksalt phase in AlN was observed at pressures as low as 1.3 GPa, as evidenced by comparing the experimental Raman spectra to calculated one- and two-phonon densities of states of the rocksalt phase.

DOI: 10.1103/PhysRevB.77.205204 PACS number(s): 62.50.−p, 63.20.−e, 78.20.Bh, 78.30.Fs

I. INTRODUCTION

Aluminum nitride (AlN) is an important semiconductor of the group III-V nitride family for the fabrication of optoelectronic devices operating in the deep UV range.[1] It crystallizes in the wurtzite structure and in the past years, there has been considerable interest in the characterization of this wide band gap semiconductor. Particular attention has been paid to the behavior under pressure of wurtzite AlN (*w*-AlN) both in bulk and nanocrystalline forms.[2–4] It has been found that *w*-AlN bulk crystals undergo a pressure-induced wurtzite-to-rocksalt phase transition near 20 GPa that is fully completed above 30 GPa, as observed by x-ray diffraction measurements.[4–7] Furthermore, theoretical studies on AlN have shown that its wurtzite structure behaves under pressure differently in comparison with other group-III nitrides, such as GaN and InN, and this leads to a different path for the wurtzite-to-rocksalt phase transition.[8,9]

The wurtzite structure has four atoms per unit cell and the group theory predicts two E_2, two B_1, one A_1, and one E_1 optical modes plus one A_1 and one E_1 acoustic modes. Figure 1 shows the atomic vibrations for each mode. The two modes with B_1 symmetry [B_1(low) and B_1(high)] are Raman forbidden, while the other four optical modes are Raman active. The crystal anisotropy of the wurtzite structure induces splitting of the A_1 and E_1 modes and the long-range Coulomb interaction splits both the A_1 and E_1 polar modes into transversal optical (TO) and longitudinal optical (LO) compo-

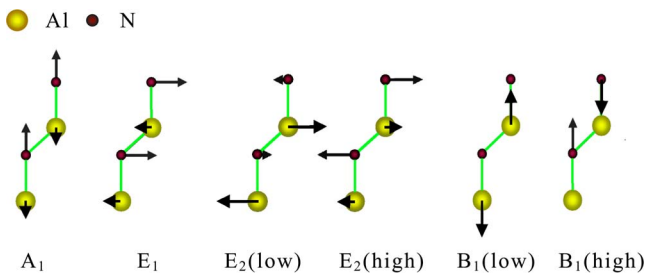

FIG. 1. (Color online) Scheme of the displacement vectors for the six different modes in *w*-AlN.

 ©2008 The American Physical Society

nents; the modes of E_2 symmetry are usually denoted E_2(low) and E_2(high). In total, there are therefore six Raman-active optical modes.

The first Raman scattering studies on *w*-AlN under pressure were performed in thin films up to 10 GPa by Sanjurjo *et al.*[10] These authors reported the pressure dependence of the TO and LO modes and the pressure coefficients of the LO-TO splitting for both the A_1 and E_1 modes; however, the E_2(high) mode was incorrectly assigned to the A_1(TO) mode. Later on, Raman scattering measurements under pressure in *w*-AlN single crystals up to 13 GPa reported estimations of the pressure coefficients of several Raman-active modes, but the LO-TO splittings were not reported.[11] More recently, Raman experiments under pressure up to 10 GPa suggested a slightly decreasing LO-TO (A_1) splitting and an increasing LO-TO (E_1) splitting with increasing pressure.[12,13] This was later confirmed in measurements of the Raman-active modes of *w*-GaN and *w*-AlN under pressures of up to 6 GPa,[14] which found a small increase in the LO-TO (E_1) splitting with increasing pressure in both materials. Finally, a very recent study reported the pressure dependence of all the Raman-active modes in *w*-AlN up to 20 GPa and showed that (i) there was a decrease in the LO-TO splitting for both A_1 and E_1 modes and (ii) there was a strong dependence of the E_2(low) mode frequency on the pressure-transmitting medium above 15 GPa.[15]

Concerning the rocksalt phase of AlN (rs-AlN), Ref. 15 is the only work, to the best of our knowledge, that has explored the experimental behavior of the Raman modes of *w*-AlN upon application of pressure up to the wurtzite-to-rocksalt phase transition. However, there is no available information regarding the behavior of the vibrational properties of AlN on decreasing pressures upon reaching the phase transition.

As regards to theoretical calculations of the lattice dynamics of *w*-AlN, full-potential linear muffin tin orbital (FP-LMTO) calculations were used to predict the frequencies and pressure coefficients of Raman-active modes, but the pressure coefficients for the LO modes were not reported.[16] *Ab initio* lattice dynamical calculations were the first to estimate the frequencies and pressure coefficients of all the Raman-active modes of *w*-AlN and predicted an increase in the LO-TO splitting for both the A_1 and E_1 modes.[17,18] Furthermore, a theoretical work was devoted to the explanation of the strange positive pressure coefficient of the E_2(low) mode in *w*-AlN.[19] Since then, several groups have performed *ab initio* lattice dynamical calculations for wurtzite and zinc blende AlN (zb-AlN) at ambient pressure[20,21] and, recently, for rs-AlN.[22] To our knowledge, there is no report on the *ab initio* calculated two-phonon density of states in any of the three phases.

In this work, we report on the pressure dependence of the Raman-active modes of wurtzite AlN up to 25 GPa, i.e., above the transition to the rocksalt structure observed here at 20 GPa. We also discuss the effect of pressure on the Raman-active modes of *w*-AlN and rs-AlN on the upstroke and the downstroke, respectively. In order to understand the pressure dependence of the phonons in the wurtzite phase and to identify the possible phases during the downstroke, we have performed *ab initio* lattice dynamical calculations of the wurtzite, zinc blende, and rocksalt phases at different pressures, including the calculation of zone-center phonons, phonon-dispersion curves, and one- and two-phonon (sum and difference) densities of states. Finally, in the light of the experimental and theoretical results, we discuss the effect of the crystal anisotropy on the pressure coefficients of the Raman modes in *w*-AlN and its comparison to those in other wurtzite semiconductors. A preliminary report on the present work using density-functional theory (DFT)–local density approximation (LDA) calculations was previously published.[23] In this work, we report a more detailed discussion on the experimental results in the light of DFT–generalized gradient approximation (GGA) calculations, which we found to be more accurate than the previous LDA calculations.

II. EXPERIMENTAL DETAILS

Wurtzite AlN single crystals of 100 μm diameter and 30 μm thickness were loaded in a diamond anvil cell equipped with 500 μm culet-size diamonds. The sample chamber was formed by drilling a 200 μm diameter hole in a 350 μm Inconel gasket that had been preindented to a thickness of 45 μm. A 4:1 methanol-ethanol mixture was used as a pressure-transmitting medium ensuring hydrostatic conditions up to 10 GPa and quasihydrostatic conditions between 10 and 20 GPa.[24] The sample pressure was determined by using a ruby chip as a pressure sensor.[25] Raman experiments at room temperature were performed in the backscattering geometry by using the 514.5 nm line of an Ar^+-ion laser and a Jobin-Yvon T64000 triple spectrometer in combination with a multichannel charge coupled device detector. The spectral resolutions were around 1 cm^{-1}. Argon and neon plasma lines were used to calibrate the spectra. The measurements were performed with a laser power below 50 mW at the sample position in order to avoid thermal effects.

III. *AB INITIO* CALCULATION DETAILS

Our calculations rely on the DFT, with a plane-wave basis set and norm-conserving pseudopotentials. We have used the ABINIT code[26–28] to calculate the structural and electronic properties, phonon frequencies, and interatomic force constants for AlN. The exchange-correlation energy was computed in the GGA by using the Perdew-Burke-Ernzerhof exchange-correlation functional.[29] The pseudopotentials were generated by using the scheme implemented in the OPIUM project[30] with *s* and *p* electrons for the valence states of both Al and N. They correspond to nonrelativistic optimized pseudopotentials obtained by following the procedure explained in Ref. 31.

To describe the electronic properties and approximate the integrals on the wave vectors of the electronic wave function over the entire first Brillouin zone (BZ), a Monkhorst-Pack grid of $10\times10\times8$ for the wurtzite and $8\times8\times8$ for the rocksalt and zinc blende unit cells[32] was used. With respect to this grid and the corresponding cutoff of 60 Ry, this choice gives an energy convergence better than 1 mhartree/f.u. and pressure accuracy of better than 0.001 GPa. The optimization of the unit cell at a given pres-

sure was performed in three steps: (i) Relaxation of the lattice parameters (a and c in the wurtzite phase and a in the zinc blende and rocksalt phases) at a given pressure with a fixed value of the internal parameter in the case of the wurtzite structure; (ii) relaxation of u at the above obtained cell parameter values; and (iii) relaxation of both the internal parameter and the lattice constants at the target pressure.

The dynamical matrices were computed by using a variational formulation of the density-functional perturbation theory.[33,34] This formulation allows the calculation of the phonon response directly from the unit cell without the use of supercells and with the possibility of calculating the dynamical matrix of an arbitrary $\boldsymbol{q}$ vector. The force constants were extracted from a Fourier transform of the dynamical matrices obtained for the predefined grid in the BZ. These matrices were then employed to obtain the phonon frequencies at arbitrary points in reciprocal space and the phonon-dispersion relations by Fourier interpolation. The one- and two-phonon densities of states were also calculated by using the same approach[35] with the initial grid and then a subsequent and increasing size was calculated until the change in the total vibrational density of states was less than 0.1.

In order to check the accuracy of our lattice dynamical calculations, Fig. 2 shows the calculated pressure dependence of the relative volume (V/V_0), the axial c/a ratio, and the internal parameter u in w-AlN. The comparison with the experimental pressure dependence of the relative volume and c/a ratio obtained from fits of data reported in the literature[5] is satisfactory. To our knowledge, no information has been reported regarding the experimental pressure dependence of the parameter u in w-AlN.

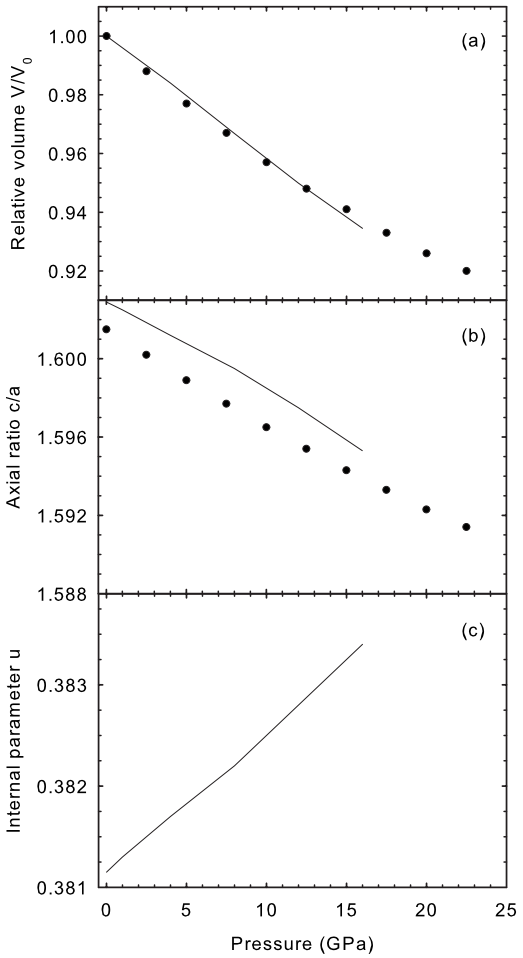

FIG. 2. Pressure dependence of the calculated structural parameters (V/V_0, c/a, and u) in w-AlN (lines). The experimental results at different pressures as obtained from fits to data of Ref. 5 are also plotted for comparison (filled circles).

IV. RESULTS AND DISCUSSION

A. Experimental and theoretical results for the wurtzite phase

Raman spectra of w-AlN at different pressures on the upstroke up to 20 GPa are shown in Fig. 3. The Raman spectra correspond to samples with good crystalline quality and display the six Raman-active modes of the wurtzite phase in order of increasing frequency: E_2(low), A_1(TO), E_2(high), E_1(TO), A_1(LO), and quasi-longitudinal-optical mode, which, for simplicity, is denoted in the following as E_1(LO). In fact, the Raman scattering of the E_1(LO) mode measured is a quasi-longitudinal-optical mode formed by the E_1(LO) mode with a slight mixture of the A_1(LO) mode.[12] The A_1(LO), E_2(low), and E_1(LO) notes can be tracked up to 9, 12, and 14 GPa, respectively. The other three Raman peaks of the wurtzite phase vanish above 18 GPa, as was already observed in Ref. 15. X-ray diffraction measurements show a wurtzite-to-rocksalt phase transition between 14 (Ref. 6) and 18 GPa (Ref. 5) and *ab initio* calculations predict the same phase transition between 8 and 13 GPa.[8,9,36–38] The disappearance of the A_1(LO) mode above 9 GPa and that of the E_2(low) mode above 12 GPa are in good agreement with the phase transition pressure estimated from theoretical calculations.

The pressure dependence of the measured and calculated phonon frequencies of the Raman-active modes in w-AlN are shown in Fig. 4. The measured and calculated zero-pressure frequencies and their pressure coefficients are summarized in Table I. The agreement between the measured and calculated values is reasonably good. The calculated frequencies slightly underestimate the experimental data, which is likely due to overestimation of the lattice parameters as is usual in DFT-GGA calculations. Also, the calculated pressure coefficients are typically 10% smaller than the experimental ones, except for the A_1(LO) mode, whose calculated pressure coefficient is 12% higher than that experimentally observed. Table I also shows the Raman frequencies and pressure coefficients obtained in previous experimental and theoretical works. In general, the agreement between the pressure coefficients of the modes reported in different experiments is rather good, with the small discrepancies possibly related to differences in sample preparation and pressure environment,[39] as was already suggested by Yakovenko *et al.*[15] For instance, the weak intensity of the A_1(TO) mode in Ref. 10 might have impacted the accuracy of the determination of its pressure coefficient, which is much smaller than the rest of the reported values for this mode.

The comparison of the different theoretical results shows reasonable agreement between our frequencies and pressure coefficients and those of previous *ab initio* calcula-

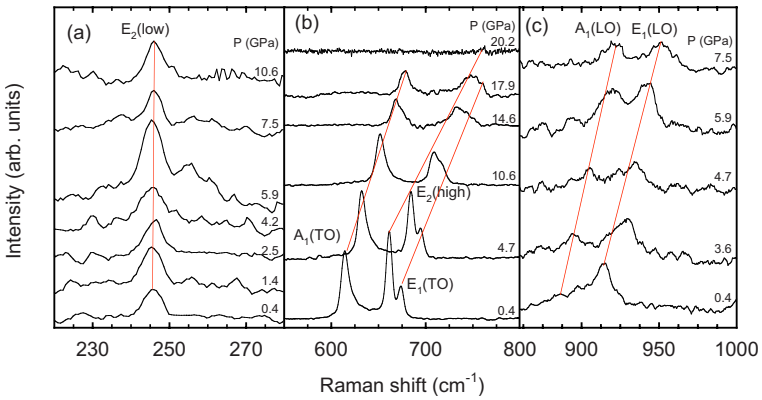

FIG. 3. (Color online) Detail of the room-temperature Raman spectra of *w*-AlN (a) in the low-frequency region up to 11 GPa, (b) in the middle-frequency region up to 20 GPa, and (c) in the high-frequency region up to 8 GPa.

tions, which were obtained with the LDA approximation.[14,17,18,20,21] In fact, our calculations closely follow the experimental data available from Raman and inelastic x-ray scatterings,[20,40] as will be shown in Sec. IV C, and the larger pressure coefficients obtained with the DFT-GGA calculations show better agreement with experimental results than the previous DFT-LDA calculations.[14,18] In this sense, several works have reported that DFT-GGA calculations are superior to DFT-LDA in calculating the lattice dynamical properties, in particular, in nitrides.[41] Only the calculated pressure coefficient of the A_1(LO) mode is more similar to the experimental one in DFT-LDA than in our DFT-GGA calculations. Although not included in Table I, the frequencies and pressure coefficients for the silent B_1(low) and B_1(high) modes were also calculated. They are 535 and 2.25 cm^{-1}/GPa for the B_1(low) mode and 707 and 3.78 cm^{-1}/GPa for the B_1(high) mode, respectively. The two calculated frequencies are in good agreement with the values of 540 and 732 cm^{-1} reported by inelastic x-ray measurements[20,40] and Raman scattering data on $Al_{1-x}Ga_xN$ samples along the full composition range,[42] respectively.

Several common trends for the measured and calculated results for *w*-AlN shown in Table I are apparent: (i) the pressure coefficient for the E_2(high) mode is similar to that of the E_1(TO) mode and (ii) the pressure coefficients for the A_1 modes are smaller than those for the E_1 modes irrespective of their transverse or longitudinal character. This increase in the A_1-E_1 splitting with pressure evidences an increase in the crystal anisotropy under compression in *w*-AlN. In this sense, it has been pointed out that the phonon frequency ratio $[\omega_{E_1(\mathrm{TO})}-\omega_{A_1(\mathrm{TO})}]/\omega_{E_1(\mathrm{TO})}$ is proportional to the structural anisotropy of a given structure.[17] For the wurtzite structure, the crystal anisotropy, $\Delta(c/a)$, is determined by the deviation of the c/a ratio from its ideal value (1.633), $\Delta(c/a)=c/a-1.633$.[43] Figure 5(a) shows the relationship between the measured $[\omega_{E_1(\mathrm{TO})}-\omega_{A_1(\mathrm{TO})}]/\omega_{E_1(\mathrm{TO})}$ phonon frequency ratio at different pressures and the crystal anisotropy $\Delta(c/a)$, as obtained from high-pressure x-ray diffraction measurements.[5] Indeed, a linear relationship is found and a fit of the experimental data (solid line) to an equation of the form

$$[\omega_{E_1(\mathrm{TO})}-\omega_{A_1(\mathrm{TO})}]/\omega_{E_1(\mathrm{TO})}=s\Delta(c/a) \quad (1)$$

yields a slope $s=1.7\pm0.2$. Figure 5(b) also illustrates the evolution of the experimental and calculated $[\omega_{E_1(\mathrm{TO})}-\omega_{A_1(\mathrm{TO})}]/\omega_{E_1(\mathrm{TO})}$ phonon frequency ratio with pressure. There seems to be a nonlinear increase in the crystal anisotropy with pressure, which is clearly underestimated in our calculations due to the larger underestimation in the pressure coefficient of the E_1(TO) mode than that of the A_1(TO) mode, despite the correct pressure dependence of the calculated c/a ratio observed in Fig. 2(b). In the following section, we will discuss that the discrepancy between the experimental and calculated pressure dependences of the crystal anisotropy may be related to the underestimation in the calculated pressure dependence of the internal parameter u.

The pressure dependence of the measured and calculated frequencies of the LO-TO splittings for the A_1 and E_1 modes in *w*-AlN is shown in Fig. 6 and summarized in Table II. Our measurements show a decreasing LO-TO splitting for both the A_1 and E_1 modes with increasing pressure and our calculations yield an increase of both LO-TO splittings with increasing pressure. The measured decrease in the LO-TO (E_1) splitting is very small and is within errors coincident with our calculations. However, the measured decrease in the LO-TO (A_1) splitting disagrees with our calculations beyond our experimental and theoretical uncertainties. These results will also be discussed in the next section. We want to stress that our experimental LO-TO splittings compare nicely to

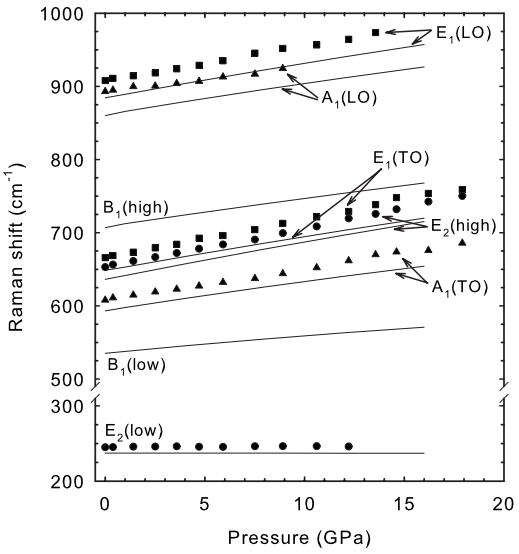

FIG. 4. Pressure dependence of the experimental (symbols) and calculated (lines) vibrational modes in *w*-AlN.

TABLE I. Zero-pressure frequencies (ω_0 in cm^{-1}) and pressure coefficients at zero pressure ($d\omega_0/dP$ in cm^{-1}/GPa) of the Raman-active optical modes of wurtzite AlN. Experimental (Expt.) and theoretical (Theor.) results are compared. Theoretical results based on the LDA or GGA formalism are also indicated in parentheses.

E_2(low)		A_1(TO)		E_2(high)		E_1(TO)		A_1(LO)		E_1(LO)		
ω_0	$d\omega_0/dP$	ω_0	$d\omega_0/dP$	ω_0	$d\omega_0/dP$	ω_0	$d\omega_0/dP$	ω_0	$d\omega_0/dP$	ω_0	$d\omega_0/dP$	Reference
245(2)	0.07(2)	608(1)	4.35(3)	653(1)	5.40(4)	666(1)	5.33(4)	893(2)	3.70(2)	908(2)	4.77(3)	Expt.[a]
		611	3.5	659.3	4.97	671.6	4.84	888	3.80	895	4.84	Expt.[b]
		610	4.08	656	5.39	669	5.07	890	4.00	911	5.51	Expt.[c]
247.5	0.12	608.5	4.40	655.5	4.99	669.3	4.55	891		910.1	4.60	Expt.[d]
249	0.05	610	4.05	657	4.78	669	4.52	890	4.00	910	3.60	Expt.[e]
241		607	4.63	660	3.99					924	1.67	Expt.[f]
237	−0.02	594	3.83	636	4.95	649	4.48	860	4.15	885	4.57	Theor. (GGA)[a]
241	−0.03	618	3.00	667	3.80	677	3.80	898	3.50	924	4.00	Theor. (LDA)[g]
236	−0.29	629	4.29	631	4.79	649	4.36					Theor. (LMTO)[h]

[a]This work.
[b]Reference 10. In this reference, the E_2(high) mode was incorrectly assigned to the A_1(TO) mode. The frequency and pressure coefficient of the real A_1(TO) mode can be estimated from the data reported in Ref. 10.
[c]References 12 and 13.
[d]Reference 14.
[e]Reference 15.
[f]Reference 11.
[g]References 14 and 18.
[h]Reference 16.

those of Yakovenko *et al.*[15] and disagree to a certain level with other experimental data summarized in Table II for comparison. From the inspection of the Raman scattering spectra reported in Refs. 10, 12, and 13, we believe that the weak intensity of some of the optical modes might have limited the accuracy of the determination of the pressure coefficients of the LO-TO splittings. Furthermore, the pressure dependence of the LO-TO (A_1) splitting in Ref. 10 was not measured since the E_2(high) mode was incorrectly assigned to the A_1(TO) mode. Unfortunately, no high-pressure Raman spectra are shown in Ref. 14, preventing a direct comparison with our spectra. The dispersion in the measured pressure coefficients of the LO-TO splittings is very high and it is difficult to draw any conclusion; however, we might point out that our negative measured pressure coefficients for both LO-TO (A_1 and E_1) splittings are in qualitative agreement with the negative values of the pressure coefficients obtained from the average of the different experimental splittings reported (−0.17 and −0.4 cm^{-1}/GPa for the A_1 and E_1 modes, respectively). Furthermore, the comparison of the experimental and theoretical results for the LO-TO splittings points out that our DFT-GGA calculations give pressure coefficients that are in better agreement with experimental results than previous DFT-LDA calculations and suggest that both LO-TO splittings in *w*-AlN have smaller pressure coefficients than those previously calculated.

B. Discussion of the results obtained for the wurtzite phase

In this section, we will show that the larger pressure coefficients of the frequencies for the E_1 modes with respect to the A_1 modes in *w*-AlN is a consequence of the increase in the crystal anisotropy with increasing pressure. The pressure dependence of the TO and LO modes in *w*-AlN is also discussed and the relative pressure coefficients of the different modes are shown to scale with the relative pressure coefficients of the two inequivalent Al-N distances of the wurtzite structure. Finally, the decrease in the LO-TO splitting for both the A_1 and E_1 modes with pressure is illustrated to be a consequence of the decrease in the bond polarizability in AlN on compression.

1. Structural anisotropy: A_1-E_1 splittings

Table III shows the pressure coefficients and the relative pressure coefficients for the Raman-active optical modes in wurtzite-type AlN, GaN, and InN. In GaN, the pressure coefficients for the A_1(TO) and E_1(TO) are very similar, thus pointing toward an almost pressure-independent A_1-E_1 (TO) splitting. Unfortunately, the only Raman measurements of InN under pressure[44] have not reported the pressure dependence of the A_1-E_1 splitting. Note that we have considered that the measured frequency of the A_1(LO) mode in InN rather correspond to the E_1(LO) (see Ref. 45). The $[\omega_{E_1(\mathrm{TO})} - \omega_{A_1(\mathrm{TO})}]/\omega_{E_1(\mathrm{TO})}$ phonon frequency ratio at ambient pressure yields 0.048, 0.061, and 0.087 for GaN, InN, and AlN, respectively.[14,46] These values qualitatively agree with the variation in $\Delta(c/a)$ in the three compounds at ambient pressure, known from structural data,[5,47] which shows that the crystal anisotropy in *w*-AlN is much larger than that in *w*-InN and that in *w*-GaN. Concerning the pressure dependence of $\Delta(c/a)$, structural data show that the crystal anisotropy is almost independent of pressure in *w*-GaN and *w*-InN,[8,47] unlike in *w*-AlN. Therefore, the large difference in

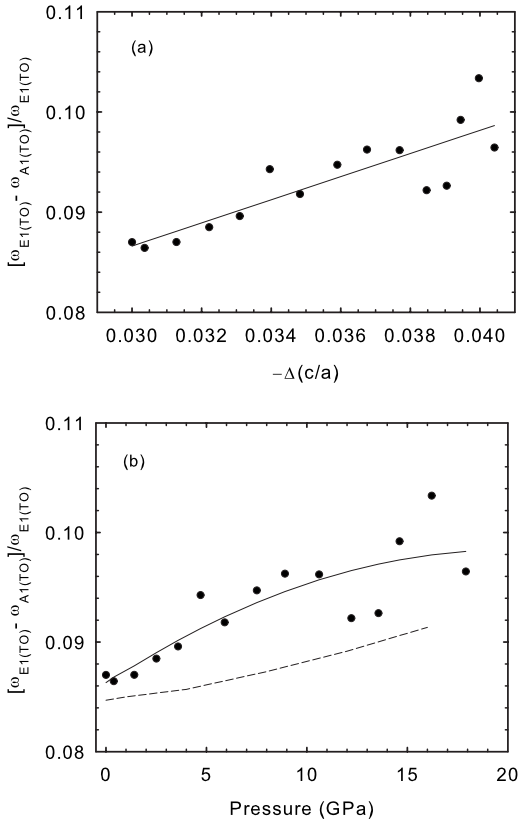

FIG. 5. (a) Dependence of the $[\omega_{E_1(\mathrm{TO})}-\omega_{A_1(\mathrm{TO})}]/\omega_{E_1(\mathrm{TO})}$ phonon frequency ratio in *w*-AlN as a function of the crystal anisotropy, $\Delta(c/a)$, as obtained from a fit of data from Ref. 5. The symbols correspond to experimental data and the solid line is a linear fit of experimental data to Eq. (1). (b) Pressure dependence of the crystal anisotropy given by the $[\omega_{E_1(\mathrm{TO})}-\omega_{A_1(\mathrm{TO})}]/\omega_{E_1(\mathrm{TO})}$ phonon frequency ratio in *w*-AlN. The symbols correspond to experimental data, the solid line is a fit of experimental data to a quadratic law, and the dashed lines correspond to calculated data.

the pressure coefficients for the E_1 and A_1 modes and the increase in the A_1-E_1 splitting for both the TO and LO modes in *w*-AlN (compared to the known values in *w*-GaN) may be related to the increase in the crystal anisotropy with increasing pressure in *w*-AlN.

In order to understand the different pressure behavior of AlN with respect to GaN and InN, the evolution under pressure of the two inequivalent nearest-neighbor bond lengths present in the wurtzite structure in *AX* compounds is analyzed. One *A*-*X* bond is along the *c* direction with bond length $R^{(1)}=uc$, with *u* being the internal parameter. The other *A*-*X* bond is in the hexagonal plane and is threefold degenerate with bond length $R^{(2)}=a\sqrt{1/3+(1/2-u)^2(c/a)^2}$. In the ideal wurtzite structure [$c/a=\sqrt{(8/3)}$ and $u=3/8$], the two bond lengths are equal and the relationship $u=a^2/(3c^2)+1/4$ between the c/a ratio and the internal parameter *u*, or equivalently, $u\cdot c/a=\sqrt{(3/8)}$, holds.[17] In real wurtzite compounds, there is always a deviation from the ideal structure and it is experimentally found that the *u* and c/a parameters are strongly correlated and that a pressure-induced decrease in the c/a ratio is accompanied by an increase in *u* according to the expression $\Delta(u)=-(3/128)^{1/2}\zeta\Delta(c/a)$, with ζ being the bond-bending parameter.[43] As a result, the variation in the relative bond lengths [$R^{(1)}(P)/R^{(1)}(0)$ and $R^{(2)}(P)/R^{(2)}(0)$] are relatively similar despite the distortion of the tetrahedral angles.[17] However, the FP-LMTO calculations found that the internal parameter *u* abnormally increased with pressure in *w*-AlN.[48] This result has been confirmed by *ab initio* calculations, like ours [see Fig. 2(c)] and those of Refs. 8 and 18, which have obtained an even larger increase in *u* with pressure than that of Ref. 48. This result implies that the relative bond length $R^{(1)}(P)/R^{(1)}(0)$ decreases with increasing pressure less quickly than the relative bond length $R^{(2)}(P)/R^{(2)}(0)$.

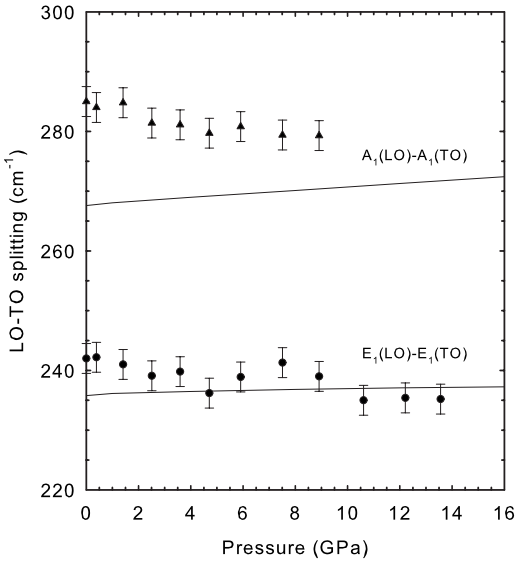

FIG. 6. Pressure dependence of the experimental (symbols) and calculated (lines) LO-TO splitting for both the A_1 and E_1 modes in *w*-AlN.

Figure 7 shows the pressure dependence of the two calculated relative bond lengths in *w*-AlN (symbols). Experi-

TABLE II. Zero-pressure LO-TO splittings and pressure coefficients in wurtzite AlN.

A_1(LO-TO)		E_1(LO-TO)		
ω_0 (cm^{-1})	$d\omega/dP$ (cm^{-1}/GPa)	ω_0 (cm^{-1})	$d\omega/dP$ (cm^{-1}/GPa)	Reference
284(3)	−0.60(5)	241(3)	−0.45(7)	Expt.[a]
277	0.30	223.4	−0.84	Expt.[b]
280	−0.10	242	0.10	Expt.[c]
		241	0.10	Expt.[d]
280	−0.30	241	−0.95	Expt.[e]
267	0.32	236	0.09	Theor. (GGA)[a]
280	0.50	247	0.21	Theor. (LDA)[f]

[a]This work.
[b]Reference 10.
[c]References 12 and 13.
[d]Reference 14.
[e]Reference 15.
[f]References 14 and 18.

TABLE III. Experimental pressure coefficients and relative pressure coefficients in wurtzite GaN, InN, and AlN. The values of AlN show the maximum reasonable dispersion values. The Grüneisen parameters can be evaluated by considering the bulk modulus of AlN (207.9 GPa) after Ref. 5, InN (125.5 GPa) after Ref. 47, and GaN (202.4 GPa) after Ref. 49.

	AlN[a]		GaN[b]		InN[c]	
Mode	$d\omega/dP$ (cm^{-1}/GPa)	$d\ln\omega/dP$ (GPa^{-1})	$d\omega/dP$ (cm^{-1}/GPa)	$d\ln\omega/dP$ (GPa^{-1})	$d\omega/dP$ (cm^{-1}/GPa)	$d\ln\omega/dP$ (GPa^{-1})
E_2(low)	0.07(1)	0.0003(1)	−0.30	−0.002		
A_1(TO)	4.35(3)	0.0070(1)	3.90	0.007	5.81	0.013
E_1(TO)	5.33(4)	0.0080(1)	3.94	0.007		
E_2(high)	5.40(4)	0.0080(1)	4.20	0.007	5.56	0.011
A_1(LO)	3.70(2)	0.0040(1)	4.40	0.006		
E_1(LO)	4.77(3)	0.0050(1)			5.96	0.010

[a]This work.
[b]Reference 14.
[c]Reference 44.

mental values are not available for *w*-AlN because the internal parameter u has not been measured under pressure to date. Neither has it been measured for *w*-GaN and *w*-InN. However, since the c/a ratio and u parameter are considered to be almost pressure independent in these two compounds,[8,47,49] the pressure dependence of the relative bond lengths in both compounds is shown in Fig. 7 for comparison because it can be calculated from the known experimental values of the c/a ratio at different pressures and from the u parameter at ambient pressure in GaN (Refs. 8 and 49) and InN.[8,47] Note that the pressure coefficients for both relative bond lengths are equal both in GaN and InN, so only one line is plotted for each compound. Furthermore, Fig. 7 shows the estimated pressure dependence of the average relative bond length in *w*-AlN, despite lack of experimental data for the bond distances in AlN under pressure, by calculating the cubic root of the experimental variation in the relative unit cell volume $V(P)/V(0)$ reported in Ref. 5 [see Fig. 2(a)]. One can observe that the average relative bond length in AlN decreases with increasing pressure at a similar rate to that of the relative bond lengths in GaN due to the similar bulk moduli of both compounds. Similarly, the pressure coefficients of the relative bond distances in InN are much higher than those in GaN and AlN due to the smaller bulk modulus (see Table III). The main result of Fig. 7 is that the pressure coefficient of the calculated relative axial bond length $R^{(1)}$ in AlN is smaller than that of the average relative Al-N bond, while that of the calculated in-plane bond length $R^{(2)}$ is larger than that of the average relative Al-N bond distance. We will show below that the different relative compressibilities of the two inequivalent Al-N bond lengths influence the different relative pressure coefficients of the Raman modes in the wurtzite structure depending on the atomic displacements for each mode.

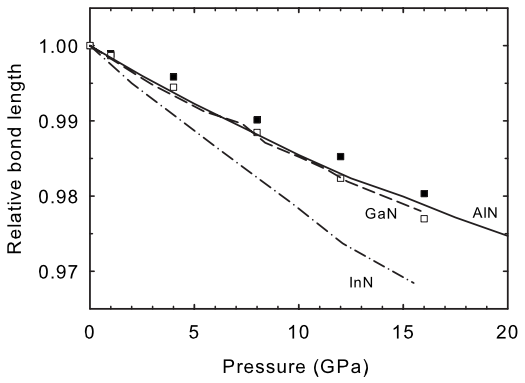

FIG. 7. Calculated relative pressure dependence of the $R^{(1)}$ (filled squares) and $R^{(2)}$ (empty squares) bond lengths in *w*-AlN. The pressure dependence of the cubic root of the relative volume of the unit cell in AlN is also depicted (dashed line) as obtained from Ref. 5. The relative pressure dependence of both bond lengths in GaN (solid line) and InN (dashed-dotted line) calculated from the known experimental values of the c/a ratio at different pressures (Refs. 46 and 48) and assuming a constant u parameter with pressure in both compounds are also shown.

2. TO modes

With regards to the TO modes, a correlation between the relative pressure coefficients of the frequency of the A_1(TO) mode (see Table III) and the bond length $R^{(1)}$ in GaN and AlN is apparent. Therefore, the similar relative pressure coefficient of the bond length $R^{(1)}$ in GaN and AlN likely accounts for the similar relative pressure coefficients of their A_1(TO) modes. This relationship comes from the fact that the TO modes under consideration are bond-stretching modes and that in the A_1 mode, the atomic displacements occur along the c axis (see Fig. 1), which is the direction of the $R^{(1)}$ bond. As shown in Table III, the relative pressure coefficients of the A_1(TO) modes in GaN and AlN are similar (0.007 GPa^{-1}) and correlate with the similar pressure coefficients for the relative bond length $R^{(1)}$ around −0.014(1) GPa^{-1} in both compounds. Furthermore, the rather large relative pressure coefficients of the A_1(TO) mode in InN (0.013 GPa^{-1}) could be explained by the much larger pressure coefficient of the relative bond length $R^{(1)}$ in InN [around −0.022(1) GPa^{-1}] than those in GaN and AlN. In the

light of the above reasoning, we suggest that the relative pressure coefficient of the A_1(TO) modes in wurtzite semiconductors is given by a phenomenological equation of the following form:

$$\frac{d \ln \omega_{\mathrm{TO}}(z)}{dP} = -\frac{1}{2}\frac{d \ln R^{(1)}}{dP}, \tag{2}$$

where we have introduced the notation $\omega_{\mathrm{TO}}(\alpha)$, with $\alpha = x,z$ referring to the frequencies of the E_1(TO) and A_1(TO) modes, respectively.

Similarly to the case of the A_1(TO) mode, the larger pressure coefficient of the in-plane relative bond length $R^{(2)}$ than that of the axial bond length $R^{(1)}$ in *w*-AlN may be responsible for the larger pressure coefficients of the E_1 modes relative to those of the A_1 modes in *w*-AlN. The correlation of the pressure coefficient of the E_1 modes with that of the in-plane relative bond length $R^{(2)}$ is also coherent with the similar relative pressure coefficients for the E_1(TO) and E_2(high) modes in *w*-AlN and also in *w*-GaN. In fact, for both these TO modes, the atomic displacements occur in the plane perpendicular to the *c* axis (see Fig. 1). This also holds for the E_2(low) mode, which, however, exhibits a completely different behavior due to the bond-bending nature of this mode. Again, Table III evidences that the relative pressure coefficients for the E_1(TO) and E_2(high) modes in AlN (0.008 GPa^{-1}) and those in GaN (0.007 GPa^{-1}) are similar and correlate with the pressure coefficients for the relative bond length $R^{(2)}$, which are around −0.016(2) and −0.014(1) in AlN and GaN, respectively. Also in InN, the measured relative pressure coefficient for the E_2(high) mode [0.011 GPa^{-1} (Ref. 44)] and for the bond length $R^{(2)}$ [−0.022(1) GPa^{-1}] obtained from Fig. 6 follow the same correlation. We anticipate that the pressure coefficient of the E_1(TO) mode in InN should be similar to that for the E_2(high) mode. As before, the relative pressure coefficient of the E_1(TO) and E_2(high) modes is −1/2 times the relative pressure coefficient of the bond length $R^{(2)}$. Consequently, the relative pressure coefficient of the E_1(TO) and E_2(high) modes in wurtzite semiconductors is given by the following quantitative correlation:

$$\frac{d \ln \omega_{\mathrm{TO}}(x)}{dP} = \frac{d \ln \omega_{E_2(\mathrm{high})}}{dP} = -\frac{1}{2}\frac{d \ln R^{(2)}}{dP}. \tag{3}$$

The validity of Eqs. (2) and (3) for the group III-nitrides and other wurtzite semiconductors is based on the fact that most of the optical modes are bond-stretching modes (see Fig. 1). It is well known that the frequency of a bond-stretching mode is proportional to the square root of the bond spring constant and inversely proportional to the square root of the reduced mass of the cation and the anion. Besides, the bond spring constant is given by the ratio of the bond force and the bond distance. With these considerations, Eqs. (2) and (3) can be obtained by differentiation with respect to the pressure *P* if one considers that the pressure dependence of the bond force *F* is negligible, as seems to be the case in wurtzite semiconductors, and that only the bond distance depends on *P*. The argument used above for deriving Eqs. (2) and (3) is also valid for LO modes. However, the behavior of the LO modes is more complicated due to the effects of the macroscopic polarization associated with them, as will be discussed later on.

Equations (2) and (3) and Fig. 7 allow us to understand the pressure dependence of the A_1-E_1 (TO) splitting in the three nitrides. In GaN and InN, the equal pressure coefficients for the relative axial and in-plane bond lengths $R^{(1)}$ and $R^{(2)}$ explain the similar relative pressure coefficients for both the A_1(TO) and E_1(TO) modes and, consequently, of their absolute pressure coefficients. In AlN, the larger pressure coefficient of the relative bond length $R^{(2)}$ compared to $R^{(1)}$ explains the larger relative and absolute pressure coefficient of the E_1(TO) compared to that of the A_1(TO) mode. The A_1-E_1(LO) splitting increases in AlN also due to the larger pressure coefficient of the E_1(LO) compared to that of the A_1(LO) mode. In fact, the smaller pressure coefficient of the A_1 modes with respect to the E_1 modes is a consequence of the increase in the internal parameter *u* with increasing pressure, which is in good agreement with theoretical calculations.[50,51]

The fact that A_1(TO) phonons in wurtzite AlN, GaN, and InN follow Eq. (2) allows us to explain the similar Grüneisen parameters, $\gamma = (B_0/\omega_0)(d\omega/dP)$, with B_0 being the bulk modulus, in the three nitrides (around 1.4 in GaN and AlN and around 1.6 in InN according to the data of this work and Refs. 14 and 44). The reason for such similarity is that the relative bond lengths in the nitrides scale with the average compressibility (or with its inverse, which is the bulk modulus); therefore, in the calculation of the Grüneisen parameter, the larger relative pressure coefficient of the TO modes in InN compared to those in AlN and GaN is counterweighted by its smaller bulk modulus, leading to a similar Grüneisen parameter in the three nitrides. In the same manner, Eq. (3) can explain the similar Grüneisen parameters of the E_1(TO) and E_2(high) modes in GaN and InN [around 1.4 (Refs. 14 and 44)], and the considerably large Grüneisen parameter (1.66) for these two modes in AlN.

The similarity of the Grüneisen parameters for the A_1(TO) modes in the three nitrides and the similarity of the Grüneisen parameters for the E_2(high) modes in GaN and InN just described indicates a close relationship between the relative pressure coefficients of the TO modes and the bulk modulus. The Grüneisen parameter of the average TO mode in nitrides can be described by the following relationship:

$$\bar{\gamma}_{\mathrm{TO}} = B_0 \frac{d \ln \bar{\omega}_{\mathrm{TO}}}{dP} \cong t, \tag{4}$$

with $t = 1.45 \pm 0.15$ being a nondimensional constant, and $\bar{\omega}_{\mathrm{TO}}$ being the average TO frequency, $\bar{\omega}_{\mathrm{TO}} = [\omega_{\mathrm{TO}}(z) + 3\omega_{\mathrm{TO}}(x)]/4$, obtained after considering that there is one cation-anion bond along the *c* axis and three in the plane perpendicular to the *c* axis. The above expression can be transformed to approximately estimate the bulk modulus in the following way:

$$\frac{1}{B_0} \cong \frac{1}{t}\left[\frac{1}{4}\frac{d \ln \omega_{\mathrm{TO}}(z)}{dP} + \frac{3}{4}\frac{d \ln \omega_{\mathrm{TO}}(x)}{dP}\right] = -\frac{1}{2t}\left[\frac{1}{4}\frac{d \ln R^{(1)}}{dP} + \frac{3}{4}\frac{d \ln R^{(2)}}{dP}\right]. \tag{5}$$

By using Eq. (5) and the relative pressure coefficients of the

TO modes in Table III, we have estimated the bulk moduli of AlN, GaN, and InN to be 200, 207, and 126 GPa, respectively. These values compare reasonably well for the three nitrides according to experimental and theoretical values summarized in Table III and reported in Refs. 8, 47, and 49. Curiously, the most striking feature of this simple calculation is that by using the same t value for the three nitrides it yields a slightly higher bulk modulus for w-GaN than for w-AlN, which is in agreement with the FP-LMTO calculations.[52] It remains to be proved whether the constants s and t in Eqs. (1) and (4), respectively, are related to each other. Note that both constants are within the estimated error interval and both are a kind of normalized frequency with respect to the crystal anisotropy and with respect to the average compressibility, respectively.

3. LO modes

As regards the LO modes, a larger relative pressure coefficient for the E_1(LO) than that for the A_1(LO) mode in w-AlN was obtained, which is in agreement with the previous discussion that accounts for a larger relative pressure coefficient of the E_1 modes than that of the A_1 modes in AlN due to the larger pressure coefficient of the relative in-plane bond distance than the relative axial bond distance. Additionally, a smaller relative pressure coefficient for the LO modes than that for the TO modes in w-AlN was determined. On the other hand, one can observe in Table III that (i) the relative pressure coefficient for the A_1(LO) mode in AlN is smaller than that in GaN, despite the similar relative pressure coefficient for the A_1(TO) mode in both compounds, and (ii) the relative pressure coefficient for the E_1(LO) in AlN is considerably smaller than that in InN. A full comparison of the LO modes in the three nitrides cannot be performed here because the pressure coefficients of the E_1(LO) mode in GaN and the A_1(LO) in InN have not been reported. However, if one considers that in GaN and InN both relative bond lengths compress at the same rate, it can be expected that similar relative pressure coefficients for the A_1(LO) and E_1(LO) modes in both GaN and InN exist.

The Lyddane-Sachs-Teller relationship $\varepsilon(\alpha)/\varepsilon_\infty(\alpha) = \omega_{\mathrm{LO}}^2(\alpha)/\omega_{\mathrm{TO}}^2(\alpha)$ for wurtzite semiconductors relates the frequency of the polar modes to the static $\varepsilon(\alpha)$ and high-frequency dielectric constants $\varepsilon_\infty(\alpha)$ for the different polarizations ($\alpha=x,z$). By using the above relationship and Eqs. (2) and (3), the relative pressure coefficients of the A_1(LO) and E_1(LO) modes in wurtzite semiconductors can be described as

$$\frac{d\ln\omega_{\mathrm{LO}}(\alpha)}{dP} = -\frac{1}{2}\frac{d\ln R^{(1,2)}}{dP} + \frac{1}{2}\frac{d\ln\varepsilon(\alpha)}{dP} - \frac{1}{2}\frac{d\ln\varepsilon_\infty(\alpha)}{dP} = -\frac{1}{2}\frac{d\ln R^{(1,2)}}{dP} + \frac{1}{2}\frac{d\ln A(\alpha)}{dP}, \quad (6)$$

with $A(\alpha)$ being a function of $\varepsilon(\alpha)$ and $\varepsilon_\infty(\alpha)$ that is related to the bond polarizability, and where the pairs ($R^{(1)}$, $\alpha=z$) and ($R^{(2)}$, $\alpha=x$) apply for the A_1(LO) and E_1(LO) modes, respectively. Equation (6) allows one to understand the smaller relative pressure coefficients of the LO modes with respect to the TO modes in AlN by considering that there is a decrease in the bond polarizability in wurtzite AlN with increasing pressure, which is similar to what occurs in most tetrahedral semiconductors.[18,53,54] It also allows one to understand that the smaller relative pressure coefficient of the A_1(LO) in AlN compared to that in GaN is related to a much larger decrease in the bond polarizability in the former than that in the latter.

As regards the LO modes in GaN and InN, the small decrease in the relative pressure coefficients of the LO modes with respect to the TO modes in GaN can be understood by a small decrease in the bond polarizability with pressure. A similar small decrease in the polarizability is expected to hold for InN on the basis of (i) the similar electronic configuration of Ga and In atoms (both with d electrons) and (ii) the similar pressure behavior of the anisotropy with increasing pressure in both compounds. The larger decrease in the bond polarizability in AlN than that in GaN and InN could be related to the increase in the crystal anisotropy with pressure in the former while the crystal anisotropy is basically constant in the latter. In this sense, Ueno *et al.*[5] noted that the decrease in the c/a ratio in AlN leads to an increase in the distortion of the tetrahedra forming the wurtzite structure, which may lead to charge transfer between the atoms in the wurtzite structure. Recent works have evidenced that the charge transfer is a general stabilization process for the wurtzite structure and is strongly coupled to geometric distortions.[55,56] The suggested charge transfer and the decrease in the bond polarizability could therefore lead to the observed decrease of the relative pressure coefficient of the E_1(LO) [A_1(LO)] mode with respect to that of the E_1(TO) [A_1(TO)] mode, which could explain the almost constant or even decreasing LO-TO splitting for both the E_1 and A_1 modes in w-AlN. In this sense, it is worth mentioning that our measured pressure dependence of the LO-TO splitting for both the A_1 and E_1 modes in w-AlN agrees with the decrease in the LO-TO splitting caused by pressure in most III-V and II-VI semiconductors.[57]

Concerning the Grüneisen parameters of the LO modes, they are similar for the A_1(LO) mode (1.2) in GaN (Ref. 14) and for the E_1(LO) mode (1.3) in InN.[44] This result is consistent with a similar negative relative pressure coefficient for the $A(\alpha)$ function in both compounds due to the similar decrease in the bond polarizability. The Grüneisen parameters of the LO modes in AlN (around 1.0) are considerably smaller than those in GaN and InN due to the larger decrease in the $A(\alpha)$ function in AlN with increasing pressure. Equation (6) also allows one to explain why in w-AlN the Grüneisen parameter of the E_1(LO) mode (1.1) is larger than that of the A_1(LO) mode (0.9), the reason being the larger pressure coefficient of the relative in-plane bond length $R^{(2)}$ than that of the relative axial bond length $R^{(1)}$.

Tables IV and V summarize the frequencies and pressure coefficients of the calculated zone center phonons of zb-AlN and rs-AlN at ambient pressure. A curious feature is that the calculated LO-TO splitting in the rocksalt phase decreases with pressure but the contrary is observed in the wurtzite and zinc blende phases. Wagner and Bechstedt[18] suggested that the reason for the increase in the LO-TO splitting in zb-AlN (and also for w-AlN and w-GaN) is the reduced screening. An increase in the LO-TO splitting with pressure was also

TABLE IV. Calculated zone-center frequencies, pressure coefficients, and LO-TO splitting in zinc blende AlN at ambient pressure.

TO		LO		LO-TO	
ω_0 (cm^{-1})	$d\omega/dP$ (cm^{-1}/GPa)	ω_0 (cm^{-1})	$d\omega/dP$ (cm^{-1}/GPa)	ω_0 (cm^{-1})	$d\omega/dP$ (cm^{-1}/GPa)
631	4.70	868	4.83	237	0.13

observed in zb-BN and zb-GaN.[10,14] Furthermore, the pressure coefficients of the LO-TO splitting in zb-BN and zb-AlN are 0.06 cm^{-1}/GPa (measured; Ref. 10) and 0.13 cm^{-1}/GPa (calculated; this work), respectively. These values seem to scale reasonably well with the bulk compressibility. In this sense, we might conjecture that the negative pressure coefficient for the LO-TO splitting measured in *w*-AlN and *w*-GaN (Ref. 58) (despite that the negative pressure coefficient in *w*-GaN was obtained from measurements in two different samples) and the positive pressure coefficient measured in zb-BN and zb-GaN, and here calculated for zb-AlN, could be related to a mechanism of charge transfer from the anion to the cation present in the wurtzite structure that might operate in a different way in the zinc blende structure. However, the charge transfer mechanism will be unclear until accurate measurements of the pressure dependence of the dielectric constants are performed.

An explanation for the slight increase in the LO-TO (A_1) splitting in our *ab initio* calculations could be the underestimation in the pressure coefficient of the u parameter in *w*-AlN, as already commented in the discussion of Fig. 5(b). Therefore, we consider that our *ab initio* calculations underestimate the pressure dependence of the internal parameter u, thus leading to overestimation of the A_1(TO) and A_1(LO) pressure coefficients and to underestimation of the E_1 and E_2(high) pressure coefficients. Furthermore, our calculations likely underestimate the pressure dependence of the charge transfer effect, leading to an even larger overestimation of the pressure coefficient of the A_1(LO) mode with respect to the A_1(TO) mode. All these effects may cause a sign reversal in the pressure coefficient of the LO-TO (A_1) splitting, thus explaining the opposite sign obtained in the calculations compared to that of the experiment.

4. Pressure dependence of the TO and LO modes in other wurtzite-type semiconductors

In this section, we would like to remark that the above equations giving the pressure behavior of the TO and LO modes in wurtzite nitrides are also valid for other wurtzite semiconductors, such as BeO and ZnO. In the former, the relative pressure coefficient for the A_1(TO) mode is around 0.008 GPa^{-1},[59] which is in good agreement with its bulk modulus (212 GPa). Furthermore, the relative pressure coefficients of the A_1(TO) and E_1(TO) modes are similar in *w*-BeO, suggesting a constant anisotropy with increasing pressure, as in the case of *w*-GaN and *w*-InN. Similarly, the relative pressure coefficient of the E_1(TO) and E_2(high) modes in *w*-ZnO are around 0.012 GPa^{-1}, which is in good agreement with its similar bulk modulus to *w*-InN.[60,61] In the case of *w*-ZnO, the DFT-LDA calculations give a larger relative pressure coefficient for the A_1(TO) mode than that for the E_1(LO) and E_2(high) modes;[62] however, the average experimental relative pressure coefficients of the Raman modes in the only two known experimental works are very similar, suggesting that the two Zn-O bond lengths $R^{(1)}$ and $R^{(2)}$ have similar relative pressure coefficients, like in *w*-GaN and *w*-InN. The controversy regarding the pressure dependence of the relative axial and in-plane Zn-O distances in *w*-ZnO is far from being resolved since several works have reported contradictory data. A rather large decrease in the c/a ratio in *w*-ZnO with pressure similar to that in *w*-AlN has been recently measured[63,64] and also an increase in the u parameter in ZnO with pressure has been calculated[65] and measured.[64] These results contrast with the small decrease in the c/a ratio and an almost constant u parameter with increasing pressure previously reported on the basis of experimental and theoretical results.[66] As regards the LO modes, a decrease in the LO-TO (A_1) splitting has been measured in *w*-BeO,[59] which is in agreement with our results for *w*-AlN; however, a small increase in the LO-TO (A_1) splitting has been measured in *w*-ZnO.[60,61] Therefore, we consider that Eqs. (1)–(6) can be applied to wurtzite oxides, but it remains to be proved whether the s and t constants in Eqs. (1) and (4) are the same for wurtzite nitrides and oxides, such as ZnO or BeO.

5. Pressure dependence of the wurtzite structure in nitrides and oxides

The different behavior under pressure of wurtzite AlN compared to GaN and InN and the mechanisms of the

TABLE V. Calculated zone-center frequencies, pressure coefficients, and LO-TO splitting in rocksalt AlN at ambient pressure.

TO		LO		LO-TO	
ω_0 (cm^{-1})	$d\omega/dP$ (cm^{-1}/GPa)	ω_0 (cm^{-1})	$d\omega/dP$ (cm^{-1}/GPa)	ω_0 (cm^{-1})	$d\omega/dP$ (cm^{-1}/GPa)
437	4.87	860	3.91	423	−0.96

wurtzite-to-rocksalt pressure-induced phase transition are in debate today. Saitta and Decremps[9] and Cai and Chen[38] suggested that this phase transition goes through different paths in the three nitrides. In AlN, the transition occurs through an intermediate hexagonal path; in GaN, it goes through an intermediate tetragonal path; and in InN, there is a controversy regarding the final mechanism of the phase transition but, initially, it goes through a tetragonal path. Saitta and Decremps[9] considered that the different paths in the three nitrides could be related to the lack of d levels in the Al cation and its presence in Ga and In; however, Cai and Chen[38] considered that the different paths can be explained in terms of ionic radii of the cations. The different path for the wurtzite-to-rocksalt phase transition in AlN with respect to those in GaN and InN is consistent with the crystallization of BN in the hexagonal graphitelike phase at ambient conditions and indicates that AlN is a compound in the borderline between the crystallization in the wurtzite or in graphitelike structure. The tendency of AlN toward the hexagonal graphitelike structure is confirmed by recent calculations in wurtzite-type binary semiconductors that have found that the highest stable number of graphitelike layers previous to their transformation in the wurtzite structure correspond to AlN.[55] In fact, the increase in the crystal anisotropy reflected in the decrease in the c/a ratio and the increase in the internal parameter u with pressure is a signature of the hexagonal intermediate phase previous to the wurtzite-to-rocksalt phase transition.[9,38,67] With this picture in mind, we can understand many of the strange properties observed in wurtzite AlN when compared to other nitrides. For instance, the small bulk modulus of AlN compared to the extrapolated value that one would obtain from the series InN-GaN-AlN is due to the small c_{11} and c_{33} elastic constants of AlN, which are similar to those of GaN.[68] The values of these elastic constants indicating softness of AlN with respect to distortions along the wurtzite c axis are related to the c_{44} elastic constant that affects the B_1(low) mode, as suggested by Saitta and Decremps.[9] In fact, our calculated pressure coefficient for the B_1(low) mode in AlN is much smaller than the rest of the optic modes at Γ with the exception of the E_2(low), which is in agreement with this picture. Similarly, the small wurtzite-to-rocksalt phase transition pressure in AlN, as compared to that in GaN, might be related to the tendency of AlN toward the graphitelike phase. On the other hand, wurtzite GaN has soft c_{44} and c_{66} elastic constants;[9] i.e., they show negative pressure coefficients due to the tendency toward a tetragonal phase on increasing pressure. The soft c_{66} elastic constant is responsible for the negative pressure coefficient of the E_2(low) mode[9] in GaN, InN, and ZnO. This is not the case for AlN, which shows a nearly zero but positive pressure coefficient, in good agreement with the calculated pressure coefficient of the c_{66} elastic constant.[9] Wurtzite BeO also exhibits positive pressure coefficients for the E_2(low) mode,[59] and the same is expected for w-SiC, so the positive pressure coefficients for the E_2(low) modes in AlN, BeO, and SiC could be related to the tendency of these semiconductors toward the intermediate hexagonal phase in the wurtzite-to-rocksalt transition in the absence of d cation levels.[9,69]

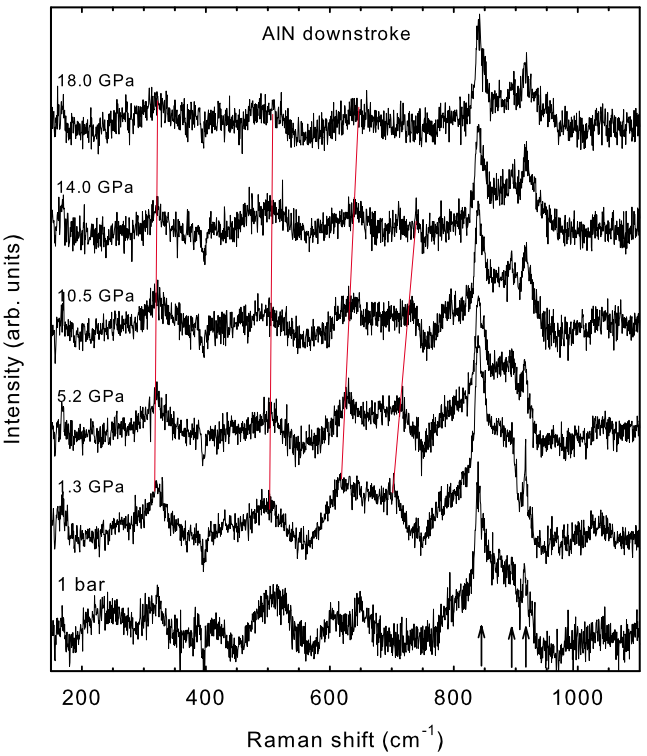

FIG. 8. (Color online) Room-temperature Raman spectra of AlN on decreasing pressure from 25 GPa. The solid lines are guides to show the behavior of certain features of the rocksalt phase. The arrows show the positions of peaks likely corresponding to the methanol-ethanol mixture.

C. High-pressure phase

On increasing pressure above 18 GPa, the Raman peaks of the wurtzite phase of AlN completely disappear and a rather flat Raman spectrum is observed up to 25 GPa. However, on decreasing pressure from 25 GPa down to ambient pressure, some features appear in the Raman spectra, especially below 14 GPa, with a progressive increase in the Raman scattering intensity of the high-pressure phase as we decrease pressure (see Fig. 8). The Raman spectra are then dominated by several peaks (marked with arrows in Fig. 8), which show no pressure dependence and that we tentatively attribute to the methanol-ethanol mixture. We point out that these bands were not observed on the upstroke but were recorded over a long integration time on the downstroke due to the small Raman intensity of the high-pressure phase. Below 14 GPa, one can distinguish three features: (1) peaks attributed to the methanol-ethanol mixture on top of a broad band that increases in intensity with decreasing pressure, (2) the observation of new bands near 300, 400, 550, and 650 cm^{-1} whose pressure dependence has been indicated with lines between 1.3 and 14 GPa, and (3) a progressive shift in the frequency of the above bands, especially the broad band centered at 650 cm^{-1} (which exhibits two maxima) at 1.3 GPa. The Raman scattering intensity of this band reaches its maximum at 1.3 GPa. The Raman spectrum at ambient pressure after releasing pressure appears rather different from that of 1.3 GPa, thus suggesting a phase transition taking place below 1.3 GPa.

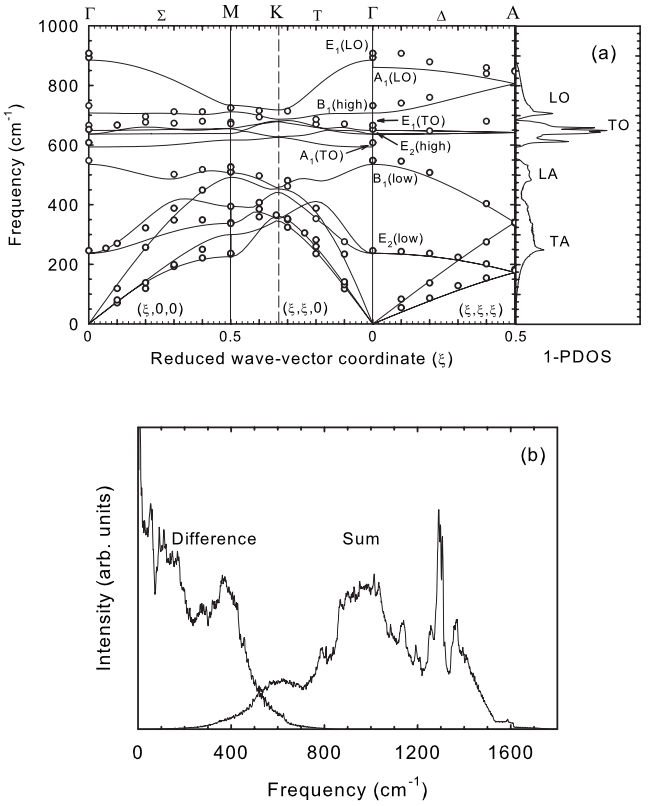

FIG. 9. *w*-AlN at ambient pressure: (a) Phonon-dispersion relations and one-phonon density of states. Experimental data are from inelastic x-ray scattering after Ref. 40. (b) Two-phonon density of states (sum and difference).

First-order Raman scattering on the rocksalt structure is symmetry forbidden. Therefore, observation of a Raman scattering signal in the rocksalt phase can be due to either second-order scattering, reflecting the two-phonon density of states (2-PDOS), which is not symmetry forbidden, or to first-order Raman scattering because of defects, reflecting the one-phonon density of states (1-PDOS) of the rocksalt phase. The 1-PDOS nature of the Raman spectra in rs-GaN (Ref. 70) and rs-InN (Refs. 44, 71, and 72) after a pressure-induced transition has been already reported. First-order Raman scattering showing the 1-PDOS can be observed after a pressure-induced transition due to defect-assisted Raman scattering (DARS); i.e., first-order Raman modes are observed because the selection rules are broken due to loss of the translational symmetry of the samples due to the excess of defects in the samples. This situation occurs after a pressure-induced transformation with a great volume collapse, like the wurtzite-rocksalt transition ($\Delta V/V_0 \sim 20\%$), because of the nanometer size of the grains in the high-pressure phase.

In order to understand the behavior of the Raman spectra in AlN after the high-pressure wurtzite-to-rocksalt phase transition, we compare the experimental Raman spectra to *ab initio* calculations of the 1-PDOS and 2-PDOS for the wurtzite, zinc blende, and rocksalt phases at different pressures. Figures 9, 10, and 11 show the phonon-dispersion curves, 1-PDOS, and 2-PDOS (sum and difference) for the wurtzite, zinc blende, and rocksalt phases of AlN at ambient pressure

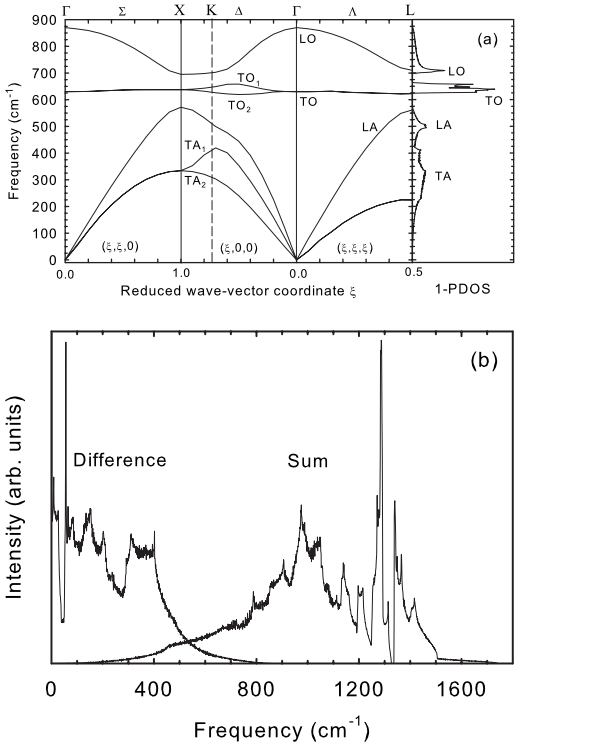

FIG. 10. zb-AlN at ambient pressure: (a) Phonon-dispersion relations and one-phonon density of states. (b) Two-phonon density of states (sum and difference).

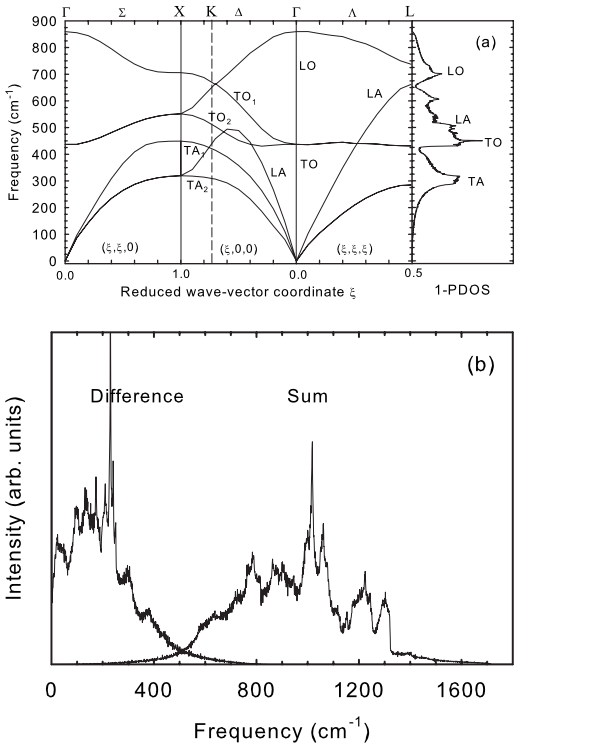

FIG. 11. rs-AlN at ambient pressure: (a) Phonon-dispersion relations and one-phonon density of states. (b) Two-phonon density of states (sum and difference).

and $T=0$ K, respectively. The phonon-dispersion curves and 1-PDOS of w-AlN are very similar to those previously reported in Refs. 15, 17, and 18, and our phonon-dispersion curves closely follow the experimental data available from Raman and inelastic x-ray scattering.[20,40] Our phonon-dispersion curves and 1-PDOS for zb-AlN are also similar to those reported by Karch and Bechstedt.[17] Finally, as regards our calculations for rs-AlN, they are similar to those recently reported;[22] however, our calculations do not show the strange dispersion of the LO phonon branch along the Γ-X and Γ-L directions present in the previous calculations.[22] The 1-PDOS of the rocksalt phase will be discussed later on; however, the 2-PDOS (difference) of the rocksalt phase is shown in Fig. 11(b) and the most significant feature is a narrow and intense peak near 220 cm^{-1}, which corresponds to the TO-TA(X) and LO-LA(X) modes near the X point of the BZ, which are located near 330 and 310 cm^{-1} in both wurtzite and zinc blende phases, respectively [see Figs. 9 and 10(b)]. Some minor contributions near 300 and 400 cm^{-1} arise from the LO-TO(L) and LO-TO(Γ) modes, respectively. Finally, contributions between 100 and 200 cm^{-1} are due to TO-LA(X-K) modes. On the other hand, the more extended 2-PDOS (sum) of the rocksalt phase also shown in Fig. 11(b) has several contributions: 2TA(X-L) modes at the X and L points of the BZ near 600 cm^{-1}; TA+TO(L) near 700 cm^{-1}; a prominent band around 760 cm^{-1} comes from the TA+TO(Γ-K-X); while the 2TO (Γ-K-X-L) modes mainly contribute to the band around 890 cm^{-1}; the peaks between 1000 and 1100 cm^{-1} are due to LA+TO(X-L) and TA+LO(X) contributions; peaks between 1100 and 1200 cm^{-1} come from the TO+LO(X-L), while that of 1230 cm^{-1} comes from LO+LA(X). Finally, the band centered around 1300 cm^{-1} is due to the TO+LO contribution near the Γ point of the BZ.

Figure 12 shows the measured Raman spectra of AlN at 1.3 GPa and at ambient pressure on decreasing pressure from 25 GPa. The spectra are compared to the calculated 1-PDOS of wurtzite and rocksalt phases at ambient pressure and with the 1-PDOS of wurtzite AlN obtained by time-of-flight neutron spectroscopy with a High-Resolution Medium-Energy Chopper Spectrometer (HRMECS-AlN) after Ref. 73. The calculated 1-PDOS for wurtzite AlN compares reasonably well with the experimental 1-PDOS if we take into account that calculated frequencies are typically 3% smaller than the experimental ones. A comparison of the experimental Raman spectra with the calculated 1-PDOS of the wurtzite, zinc blende, and rocksalt phases suggests that the Raman spectrum at 1.3 GPa is rather similar to the 1-PDOS of the rocksalt structure, whereas the Raman spectrum at ambient pressure resembles the calculated and measured 1-PDOS of the wurtzite structure.[73,74]

In order to interpret the Raman spectra of the rocksalt phase of AlN, there are several clear features in the Raman spectrum at 1.3 GPa in Fig. 12. One is the marked peak near 300 cm^{-1}, which is attributed to the contributions from the transverse acoustic branch along the X-L direction of the rocksalt phase. Another is the broad band between 400 and 550 cm^{-1}, which may correspond to the contribution of the LA(X) and TO(Γ-L) modes of the rocksalt phase. The last one is the broad band between 550 and 750 cm^{-1}, which

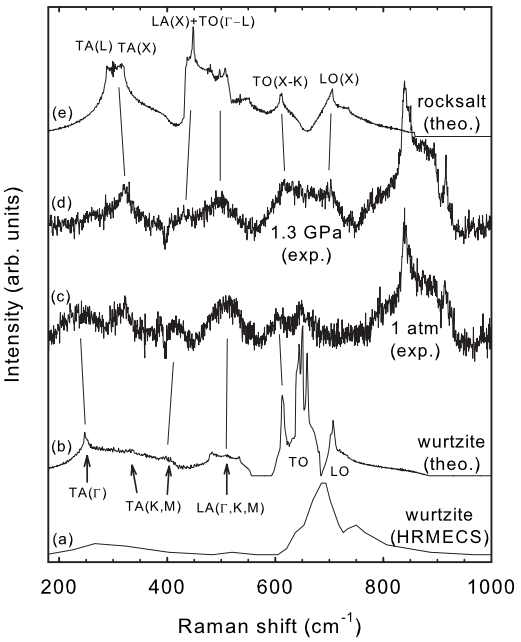

FIG. 12. (a) Comparison of the 1-PDOS of w-AlN measured by HRMECS after Ref. 73; (b) the 1-PDOS of w-AlN calculated at 1 atm; the experimental Raman spectrum on the downstroke at (c) 1 atm and at (d) 1.3 GPa; and (e) the 1-PDOS of rs-AlN calculated at 1 atm. The lines are guides for the comparison among the different peaks.

stems from the TO(W) region of the rocksalt phase (low-frequency maximum) and from the contribution of the LO(X) region of the rocksalt phase (high-frequency maximum). The measured pressure coefficients for the broad bands discussed here are considerably smaller than those of the nearest bands in the 1-PDOS of the wurtzite phase and much closer in value to those calculated for the rocksalt phase. However, at present, the reason for the large discrepancy between the measured pressure coefficients and the calculated ones that are summarized in Table VI is not known. Contributions of second-order features of the rocksalt phase to the experimental Raman spectrum have not been clearly observed.

Features of the wurtzite phase in the experimental Raman spectrum at ambient pressure can be similarly interpreted. In

TABLE VI. Measured and calculated frequencies and pressure coefficients in rocksalt AlN at 1.3 GPa on decreasing pressure. Tentative assignments are also included.

Experimental		Theoretical		
ω_0 (cm^{-1})	$d\omega/dP$ (cm^{-1}/GPa)	ω_0 (cm^{-1})	$d\omega/dP$ (cm^{-1}/GPa)	Assignment
300	0.30	300	1.66	TA(X)
500	1.50	450	2.90	LA(X)
		500	4.40	TO(Γ-L)
620	2.50	620	4.20	TO(X-K)
700	2.60	710	3.80	LO(X)

this Raman spectrum, the broad bands around 250 and 500 cm^{-1} correlate with the maxima of the 1-PDOS corresponding to the TA(Γ) and the LA(Γ-*K*-*M*) modes of the wurtzite phase. Finally, the two marked maxima of the band that extends from 550 to 700 cm^{-1} can be assigned to contributions of the TO branches since the contribution of the LO branches are considerably smaller. Therefore, we conclude from the comparison between experimental and theoretical data that the rocksalt phase in AlN is preserved down to 1.3 GPa on decreasing pressure and that there is a partial transformation to the wurtzite phase below 1.3 GPa. This result seems to contradict the previous experiments that quenched the rocksalt phase after a high-pressure treatment;[6,75] however, it agrees with the rocksalt-to-wurtzite backtransformation found in InN.[44] This backtransformation to the wurtzite phase in AlN can be understood if we consider that the full wurtzite-to-rocksalt phase transition is only completed above 30 GPa (Ref. 4) and that we have only reached a pressure of 25 GPa in our experiments. Therefore, some microcrystals or nanocrystals of the wurtzite phase could remain at 25 GPa, which leads to nucleation of this phase on decreasing pressure. As regards the band near 320 cm^{-1} in the spectrum at ambient pressure, it can come either from rests of the rocksalt phase or from the difference TO-TA second-order mode of the wurtzite phase already present at ambient pressure. We can also note that the increasing contribution of the 1-PDOS of the rocksalt phase in AlN with decreasing pressure is in agreement with the backtransformation to the wurtzite phase. As pressure decreases below 14 GPa, there is a gradual increase in the intensity of the Raman scattering due to DARS of the rocksalt phase likely due to progressive transformation of the sample from the rocksalt to the wurtzite structure. Finally, we can mention that the wurtzite-to-rocksalt transition measured on the upstroke at 18 GPa and on the downstroke below 1.3 GPa indicate that the middle of the hysteresis cycle is somewhat below 9.6 GPa. This value is in good agreement with the pressure of the coexistence of both phases (9.2 GPa) reported by Serrano *et al.*[8]

V. CONCLUSIONS

We have performed Raman scattering measurements in *w*-AlN at room temperature up to 25 GPa. The pressure dependence of the phonon frequencies of AlN in the wurtzite and high-pressure phases are reported and compared to *ab initio* lattice dynamical calculations performed for the wurtzite, zinc blende, and rocksalt phases. Our theoretical results using DFT-GGA calculations show pressure coefficients for wurtzite-type modes that are in better agreement with experimental Raman data than previous calculations. We have measured much larger pressure coefficients for the E_1 and E_2(high) modes in *w*-AlN than for the A_1 modes. This result is a consequence of the bond-stretching nature of the modes and of the different compressibilities of the two inequivalent Al-N bond distances in the wurtzite structure. We have shown that the relative pressure coefficients of the TO modes in wurtzite materials scale with the relative compressibility of their cation-anion distances. Furthermore, we consider that the relatively small bulk modulus and phase transition pressure as well as the counterintuitive positive pressure coefficient of the E_2(low) in *w*-AlN are consequences of the tendency of the wurtzite AlN structure toward the hexagonal graphitelike structure of BN with increasing pressure previous to the wurtzite-to-rocksalt phase transition. The tendency toward the graphitelike structure in *w*-AlN is manifested through a decrease in the c/a ratio and the increase in the internal parameter u under compression. This tendency toward an intermediate hexagonal phase in *w*-AlN is contrary to that of other wurtzite semiconductors, such as GaN and InN, which tend to an intermediate tetragonal phase and show a pressure-independent anisotropy and, consequently, similar relative pressure coefficients for the E_1 and A_1 modes.

We have measured a negative pressure coefficient for the LO-TO splitting for both the A_1 and E_1 modes in *w*-AlN that curiously agrees with the average of the pressure coefficients reported in the literature. The decrease in the LO-TO splitting is attributed to a decrease in the ionicity of AlN under compression. Our theoretical results for the LO-TO splittings do not agree with the experimental data but the deviation is within errors in the case of the LO-TO (E_1) splitting. The discrepancies may be related to the underestimation of the pressure coefficient of the internal parameter u in the calculations and deviations regarding the pressure dependence of the charge transfer. Curiously enough, the calculations predict an increase in the LO-TO splitting in zb-AlN, which is in agreement with the predictions for other nitrides. It remains to be proved whether the increase or decrease in the LO-TO splitting with increasing pressure in nitrides and other semiconductors with anions of the first row (C, N, and O) is related to the different behaviors of the bonds under pressure in the zinc blende and wurtzite structures.

Finally, we have observed a weak Raman scattering appearing below 14 GPa on decreasing pressure from 25 GPa and lasting down to 1.3 GPa. Such Raman scattering has been attributed to the one-phonon density of states of the rocksalt phase. Below 1.3 GPa, there is a partial return to a disordered wurtzite phase likely due to its nucleation from wurtzite microcrystals still present at 25 GPa due to the incomplete wurtzite-to-rocksalt phase transition.

ACKNOWLEDGMENTS

This work was supported by the Spanish MCYT (Projects No. MAT2006-02279, No. MAT2007-65990-C03-01, and No. MAT2007-60087), by Generalitat Valenciana (Projects No. GV06/358 and No. ACOMP06/81), and by Generalitat de Catalunya (Grants No. 2005SGR00535 and No. 2005SGR201). The authors thank J. H. Edgar (Kansas State University) for supplying the AlN samples, A. Cantarero for providing access to the experimental Raman setup, and A. Segura for critical reading of the manuscript. D.E. acknowledges the financial support from the MEC of Spain through the "Ramón y Cajal" program. A.H.R. is supported by Project No. J-59853-F from CONACYT-Mexico. We would also like to thank the Centro Nacional de Spercomputo at IPICyT, Mexico for allocation of computer time.

*Corresponding author; fjmanjon@fis.upv.es

[1] J. Li, Z. Y. Fan, R. Dahal, M. L. Nakarmi, J. Y. Lin, and H. X. Jiang, Appl. Phys. Lett. **89**, 213510 (2006).
[2] Z. Wang, K. Tait, Y. Zhao, D. Schiferl, C. Zha, H. Uchida, and R. Downs, J. Phys. Chem. B **108**, 11506 (2004).
[3] P. S. Branicio, R. K. Kalia, A. Nakano, and P. Vashishta, Phys. Rev. Lett. **96**, 065502 (2006).
[4] L. H. Shen, X. F. Li, Y. M. Ma, K. F. Yang, W. W. Lei, Q. L. Lui, and G. T. Zou, Appl. Phys. Lett. **89**, 141903 (2006).
[5] M. Ueno, A. Onodera, O. Shimomura, and K. Takemura, Phys. Rev. B **45**, 10123 (1992).
[6] Q. Xia, H. Xia, and A. L. Ruoff, J. Appl. Phys. **73**, 8198 (1993).
[7] S. Uehara, T. Masamoto, A. Onodera, M. Ueno, O. Shinomura, and K. Takemura, J. Phys. Chem. Solids **58**, 2093 (1997).
[8] J. Serrano, A. Rubio, E. Hernández, A. Muñoz, and A. Mujica, Phys. Rev. B **62**, 16612 (2000).
[9] A. M. Saitta and F. Decremps, Phys. Rev. B **70**, 035214 (2004).
[10] J. A. Sanjurjo, E. López-Cruz, P. Vogl, and M. Cardona, Phys. Rev. B **28**, 4579 (1983).
[11] P. Perlin, A. Polian, and T. Suski, Phys. Rev. B **47**, 2874 (1993).
[12] M. Kuball, J. M. Hayes, A. D. Prins, N. W. A. van Uden, D. J. Dunstan, Y. Shi, and J. H. Edgar, Appl. Phys. Lett. **78**, 724 (2001).
[13] M. Kuball, J. M. Hayes, Y. Shi, J. H. Edgar, A. D. Prins, N. W. A. van Uden, and D. J. Dunstan, J. Cryst. Growth **231**, 391 (2001).
[14] A. R. Goñi, H. Siegle, K. Syassen, C. Thomsen, and J.-M. Wagner, Phys. Rev. B **64**, 035205 (2001).
[15] E. V. Yakovenko, M. Gauthier, and A. Polian, JETP **98**, 981 (2004).
[16] I. Gorczyca, N. E. Christensen, E. L. Peltzer y Blancá, and C. O. Rodríguez, Phys. Rev. B **51**, 11936 (1995).
[17] K. Karch and F. Bechstedt, Phys. Rev. B **56**, 7404 (1997).
[18] J.-M. Wagner and F. Bechstedt, Phys. Rev. B **62**, 4526 (2000).
[19] J.-M. Wagner and F. Bechstedt, Phys. Status Solidi B **235**, 464 (2003).
[20] M. Schwoerer-Böhning, A. T. Macrander, M. Pabst, and P. Pavone, Phys. Status Solidi B **215**, 177 (1999).
[21] C. Bungaro, K. Rapcewicz, and J. Bernholc, Phys. Rev. B **61**, 6720 (2000).
[22] A. Siegel, K. Parlinski, and U. D. Wdowik, Phys. Rev. B **74**, 104116 (2006).
[23] F. J. Manjón, D. Errandonea, N. Garro, A. H. Romero, J. Serrano, and M. Kuball, Phys. Status Solidi B **244**, 42 (2007).
[24] G. J. Piermarini, S. Block, and J. D. Barnett, J. Appl. Phys. **44**, 5377 (1973).
[25] G. J. Piermarini, S. Block, J. D. Barnett, and R. A. Forman, J. Appl. Phys. **46**, 2774 (1975).
[26] X. Gonze, J.-M. Beuken, R. Caracas, F. Detraux, M. Fuchs, G.-M. Rignanese, L. Sindic, M. Verstraete, G. Zerah, F. Jollet, M. Torrent, A. Roy, M. Mikami, Ph. Ghosez, J.-Y. Raty, and D. C. Allan, Comput. Mater. Sci. **25**, 478 (2002).
[27] X. Gonze, G.-M. Rignanese, M. Verstraete, J.-M. Beuken, Y. Pouillon, R. Caracas, F. Jollet, M. Torrent, G. Zerah, M. Mikami, P. Ghosez, M. Veithen, J. Y. Raty, V. Olevano, F. Bruneval, L. Reining, R. Godby, G. Onida, D. R. Hamann, and D. C. Allan, Z. Kristallogr. **220**, 558 (2005).
[28] The ABINIT code is a common project of the Université Catholique de Louvain, Corning Incorporated, and other contributors (http://www.abinit.org).
[29] J. P. Perdew, K. Burke, and M. Ernzerhof, Phys. Rev. Lett. **77**, 3865 (1996).
[30] http://opium.sourceforge.net/
[31] A. M. Rappe, K. M. Rabe, E. Kaxiras, and J. D. Joannopoulos, Phys. Rev. B **41**, 1227 (1990).
[32] H. J. Monkhorst and J. D. Pack, Phys. Rev. B **13**, 5188 (1976).
[33] X. Gonze, Phys. Rev. B **55**, 10337 (1997).
[34] X. Gonze and C. Lee, Phys. Rev. B **55**, 10355 (1997).
[35] S. Baroni, P. Giannozzi, and A. Testa, Phys. Rev. Lett. **58**, 1861 (1987).
[36] C. C. Silva, H. W. Leite Alves, L. M. R. Scolfaro, and J. R. Leite, Phys. Status Solidi C **2**, 2468 (2005).
[37] A. Muñoz and K. Kunc, Phys. Rev. B **44**, 10372 (1991).
[38] J. Cai and N. Chen, Phys. Rev. B **75**, 134109 (2007).
[39] D. Errandonea, Y. Meng, M. Somayazulu, and D. Hausermann, Physica B **355**, 116 (2005).
[40] M. Schwoerer-Böhning and A. T. Macrander, J. Phys. Chem. Solids **61**, 485 (2000).
[41] A. Zoroddu, F. Bernardini, P. Ruggerone, and V. Fiorentini, Phys. Rev. B **64**, 045208 (2001).
[42] V. Yu. Davydov, I. N. Goncharuk, A. N. Smirnov, A. E. Nikolaev, W. V. Lundin, A. S. Usikov, A. A. Klochikhin, J. Aderhold, J. Graul, O. Semchinova, and H. Harima, Phys. Rev. B **65**, 125203 (2002).
[43] P. Lawaetz, Phys. Rev. B **5**, 4039 (1972).
[44] C. Pinquier, F. Demangeot, J. Frandon, J.-C. Chervin, A. Polian, B. Couzinet, P. Munsch, O. Briot, S. Ruffenach, B. Gil, and B. Maleyre, Phys. Rev. B **73**, 115211 (2006).
[45] Z. G. Qian, W. Z. Shen, H. Ogawa, and Q. X. Guo, J. Phys.: Condens. Matter **16**, R381 (2004).
[46] V. Yu. Davydov, V. V. Emtsev, I. N. Goncharuk, A. N. Smirnov, V. D. Petrikov, V. V. Mamutin, V. A. Vekshin, S. V. Ivanov, M. B. Smirnov, and T. Inushima, Appl. Phys. Lett. **75**, 3297 (1999); V. Yu. Davydov, A. A. Klochikin, M. B. Smirnov, V. V. Emtsev, V. D. Petrikov, I. A. Abroyan, A. I. Titov, I. N. Goncharuk, A. N. Smirnov, V. V. Mamutin, S. V. Ivanov, and T. Inushima, Phys. Status Solidi B **216**, 779 (1999).
[47] M. Ueno, M. Yoshida, A. Onodera, O. Shimomura, and K. Takemura, Phys. Rev. B **49**, 14 (1994).
[48] N. E. Christensen and I. Gorczyca, Phys. Rev. B **47**, 4307 (1993).
[49] T. Tsuchiya, K. Kawamura, O. Ohtaka, H. Fukui, and T. Kikegawa, Solid State Commun. **121**, 555 (2002).
[50] J.-M. Wagner and F. Bechstedt, Phys. Status Solidi B **216**, 793 (1999).
[51] H. M. Tütüncü and G. P. Srivastava, Phys. Rev. B **62**, 5028 (2000).
[52] K. Kim, W. R. L. Lambrecht, and B. Segall, Phys. Rev. B **53**, 16310 (1996).
[53] T. Sengstag, N. Binggeli, and A. Baldereschi, Phys. Rev. B **52**, R8613 (1995).
[54] S. Q. Wang and H. Q. Ye, J. Phys.: Condens. Matter **17**, 4475 (2005), and references therein.
[55] A. Wander, F. Schedin, P. Steadman, A. Norris, R. McGrath, T. S. Turner, G. Thornton, and N. M. Harrison, Phys. Rev. Lett. **86**, 3811 (2001).
[56] C. L. Freeman, F. Claeyssens, N. L. Allan, and J. H. Harding, Phys. Rev. Lett. **96**, 066102 (2006).
[57] M. D. Frogley, D. J. Dunstan, and W. Palos, Solid State Commun. **107**, 537 (1998).

[58] P. Perlin, T. Suski, J. W. Ager, G. Conti, A. Polian, N. E. Christensen, I. Gorczyca, I. Grzegory, E. R. Weber, and E. Haller, Phys. Rev. B **60**, 1480 (1999).
[59] A. P. Jephcoat, R. J. Hemley, H. K. Mao, R. E. Cohen, and M. J. Mehl, Phys. Rev. B **37**, 4727 (1988).
[60] F. J. Manjón, K. Syassen, and R. Lauck, High Press. Res. **22**, 299 (2002).
[61] F. Decremps, J. Pellicer-Porres, A. M. Saitta, J. C. Chervin, and A. Polian, Phys. Rev. B **65**, 092101 (2002).
[62] J. Serrano, A. H. Romero, F. J. Manjón, R. Lauck, M. Cardona, and A. Rubio, Phys. Rev. B **69**, 094306 (2004).
[63] H. Sowa and H. Ahsbahs, J. Appl. Crystallogr. **39**, 169 (2006).
[64] H. Liu, Y. Ding, M. Somayazulu, J. Qian, J. Shu, D. Häusermann, and H. K. Mao, Phys. Rev. B **71**, 212103 (2005).
[65] J. E. Jaffe and A. C. Hess, Phys. Rev. B **48**, 7903 (1993).
[66] F. Decremps, F. Datchi, A. M. Saitta, A. Polian, S. Pascarelli, A. Di Cicco, J. P. Itié, and F. Baudelet, Phys. Rev. B **68**, 104101 (2003).
[67] S. Limpijumnong and W. R. L. Lambrecht, Phys. Rev. Lett. **86**, 91 (2001); Phys. Rev. B **63**, 104103 (2001).
[68] D. K. Pandey, D. Singh, and R. P. Yadav, Appl. Acoust. **68**, 766 (2007).
[69] M. Durandurdu, Phys. Rev. B **75**, 235204 (2007).
[70] M. P. Halsall, P. Harmer, P. J. Parbrook, and S. J. Henley, Phys. Rev. B **69**, 235207 (2004).
[71] C. Pinquier, F. Demangeot, J. Frandon, J. W. Pomeroy, M. Kuball, H. Hubel, N. W. A. van Uden, D. J. Dunstan, O. Briot, B. Maleyre, S. Ruffenach, and B. Gil, Phys. Rev. B **70**, 113202 (2004).
[72] C. Pinquier, F. Demangeot, J. Frandon, O. Briot, B. Maleyre, S. Ruffenach, B. Gil, J. W. Pomeroy, M. Kuball, H. Hubel, N. W. A. van Uden, and D. J. Dunstan, Superlattices Microstruct. **36**, 581 (2004).
[73] J. C. Nipko and C.-K. Loong, Phys. Rev. B **57**, 10550 (1998).
[74] V. Yu. Davydov, Yu. E. Kitaev, I. N. Goncharuk, A. N. Smirnov, J. Graul, O. Semchinova, D. Uffmann, M. B. Smirnov, A. P. Mirgorodsky, and R. A. Evarestov, Phys. Rev. B **58**, 12899 (1998).
[75] H. Vollstädt, E. Ito, M. Akaishi, S. Akimoto, and O. Fukunaga, Proc. Jpn. Acad., Ser. B: Phys. Biol. Sci. **66**, 7 (1990).